Multiscale Simulations of Carbon-Based Composites for the Design of Sustainable Automotive Parts

Kostantinos Margaronis[1], Vasileios Merevis[1], Rahul Banerjee[2(✉)], Ioannis Kalogeris[1], Philippe Mauri[2], Arijit Mallick[2], Stefanos Pyrialakos[1], Vissarion Papadopoulos[1], Martin Obstbaum[2], and Victor Faessler[2]

[1] MGroup, Engineering Simulations Lab, Institute of Structural Analysis and Antiseismic Research, National University of Athens, Zografou, Greece
[2] TWT GmbH Science & Innovation, Stuttgart, Germany
{rahul.banerjee,controlling}@twt-gmbh.de

Abstract. Energy absorption during an impact is very important in a vehicle's bumper system. This work aims to study the improvement of energy absorption and intrusion characteristics of bumpers made of carbon nanotube-reinforced polymers in comparison with conventional materials used in the automotive industry. A parametric investigation is conducted by simulation of impact using contact finite element methods, while the composite material is modeled using multiscale methods, based on computational homogenization. The immense computational requirements associated with the aforementioned methods are addressed by a surrogate modeling technique, which utilizes neural networks, trained to predict the nonlinear stress-strain relationship of the composite. The obtained results suggest that the energy absorption of the bumper system increases significantly for the bumpers made of reinforced polymer. Our future goal is to deploy this model on exascale HPC systems for performing material optimization to find the optimal material configurations that will maximize the vehicle's crashworthiness.

Keywords: Impact simulation · Composite bumper structure · Contact finite elements · Carbon nanotubes · Reinforced polymer · Surrogate model · Multiscale analysis · Neural networks · Machine learning

© Der/die Autor(en): exklusiv lizenziert an Springer Fachmedien Wiesbaden GmbH, ein Teil von Springer Nature 2023
A. C. Kulzer et al. (Hrsg.): ISSYM 2023 Proceedings, S. 187–201, 2023.
https://doi.org/10.1007/978-3-658-42236-3_14

1 Introduction

The growing socioeconomic concerns on transport safety and fuel consumption have made the need for designing lighter and crashworthy structures more and more recognized. In the automotive industry, structural crashworthiness, which refers to the vehicle's response as it undergoes impact, is an important requirement in the design of vehicle parts, as it is essential to increase the safety of passengers in such scenarios. For instance, the car bumper system plays a major role in enhancing safety for both passengers and pedestrians, by absorbing maximum kinetic energy and minimizing damage to vulnerable parts of the vehicles in cases of impact. At the same time, rapid motorization has made lightweighting of the vehicle imperative due to concerns in energy consumption and environment.

For these reasons, there has been a growing interest in crashworthiness research and development over the recent years with particular emphasis on innovative material solutions that combine increased crashworthiness with lightweighting [1,2]. These include fiber reinforced composite materials such as E- Glass/Epoxy bidirectional laminates [3], glass mat thermoplastic with short glass fibers [4] and kenaf/glass fibers [5]. In all cases, the addition of fibers in the polymer resulted in improved mechanical properties (tensile strength, flexural modulus and strength), but the impact properties of the composite remained inadequate.

As an alternative to natural fibers, polymer composites reinforced with carbon nanotubes (CNTs) have been also considered as high-performing materials for the development of vehicle parts. Over the last few decades, CNTs have been widely used in the polymer material industry due to their superior mechanical and physical properties, as they are characterized by outstanding thermal [6] and electrical properties [7], high Young's modulus [8] and low density, making them ideal for high-performance multifibres and composites. In structural applications their incredible strength and nano-dimensions make CNTs unique as mechanical reinforcements. In addition, CNT-reinforced composites are characterized by good impact properties such as impact toughness, impact strength and interlaminar shear strength [9,10]. This is attributed to the CNTs' ability to absorb more impact energy compared to the unreinforced polymer, contributing to a remarkable improvement in impact strength. The high energy absorption of CNT-reinforced polymers along with their low density and increased strength, stiffness and fracture resistance [11,12] make them excellent candidates for vehicle parts.

Even though CNTs have the potential to create high performance composites, yet, the large amount of resources required for experimental studies of their behavior hinders the progress on this field. A promising approach to overcome this problem is by using computational approaches that will enable researchers to study a large number of material combinations and microstructural configurations with marginal investment in terms of money, time and labor. However, the development of accurate numerical models for nano-reinforced composites is a very challenging problem in the field of computational mechanics due to

the increased complexity of modeling the various physical laws governing the problem at different length scales [13,14].

In this work, a computational model is developed for characterizing the mechanical behavior of CNT-reinforced polymers, based on the concept of computational homogenization [15]. In particular, the composite material's constitutive law is obtained through the analysis of a representative volume element (RVE) of the composite material under various loading conditions and averaging over the field variables of the RVE. Next, the FE^2 technique [16] is employed in order to study the response of a car bumper made up from the composite. Despite its accuracy, FE^2 is associated to extreme computational costs as it requires the solution of the RVE boundary value problem at each integration point in the finite element model of the bumper. To overcome this issue, surrogate models of the RVE were developed using artifical neural networks that were trained to emulate the RVE's nonlinear stress-strain relation, as proposed in [17,18]. Lastly, a contact finite element formulation is developed, which is coupled with the FE^2 scheme in order to perform impact analysis on the bumper. A parametric investigation is then performed to assess its crashworthiness for the case of $1.0wt.\%$ CNT-reinforcement in the polymeric matrix.

The paper is organized as follows. Section 2 revisits the fundamentals of impact theory and introduces the numerical tools for impact simulation, focusing on the discretization of a contact interface using the finite element method. Section 3 presents a computational framework based on the FE^2 method for studying the behavior of systems made from CNT-reinforced composites. This section also describes a surrogate modeling technique based on neural networks to drastically reduce the computational cost of the problem. Section 4 provides a numerical application of a rear truck bumper made of CNT-reinforced polymer and compares its performance in terms of energy absorption with conventional bumper materials. Lastly, in Sect. 5 the concluding remarks and future research directions are discussed.

2 Numerical Model

This section presents the spatial discretization and time discretization methods used in this work in order to study the dynamic response of a solid body, and in particular a car bumper, during impact.

2.1 Spatial Discretization

The weak formulation which describes the spatial and structural interaction of the two bodies that come in contact is presented in Eq. (1). The first part in brackets describes the structural problem and the last part of the equation describes the contact interface problem.

$$\sum_{\beta=1}^{2}\left\{\int_{V^\beta}\boldsymbol{S}\cdot\delta\boldsymbol{E}dV-\int_{V^\beta}\boldsymbol{b}\cdot\delta\boldsymbol{u}dV-\int_{A_\sigma^\beta}\boldsymbol{t}\cdot\delta\boldsymbol{u}dA\right\}+\int_{\Gamma_c}e_N g_n\delta g_n d\Gamma=0 \quad (1)$$

where $\boldsymbol{S}$ is the second Piola stress tensor, $\boldsymbol{E}$ the Green strain tensor, $\boldsymbol{b}$ the body forces, $\boldsymbol{t}$ the tractions, $\boldsymbol{u}$ the displacement vector, e_N the interface stiffness and g the gap function.

For the spatial discretization, the finite element method was implemented using two types of elements. An 8-node hexaedral element based on the Solid-Shell formulation [19] was used to discretize the solid bodies. To capture the interfacial interactions between the two solid bodies a 8-node contact element was used based on Surface to Surface formulation.

The matrix formulation of the structural part of Eq. (1) is given in Eqs. (2) and (3), for the stiffness matrix and the residual vector respectively.

$$\boldsymbol{K}_{solid} = \boldsymbol{K}_{uu} - \boldsymbol{K}_{au}^T \boldsymbol{K}_{aa}^{-1} \boldsymbol{K}_{au} \tag{2}$$

$$\boldsymbol{R}_{solid} = \boldsymbol{F}_{ext} - \boldsymbol{F}_{int} + \boldsymbol{K}_{au}^T \boldsymbol{K}_{aa}^{-1} \boldsymbol{F}_{enh} \tag{3}$$

where $\boldsymbol{K}_{uu}$, $\boldsymbol{K}_{au}$, $\boldsymbol{K}_{aa}$, $\boldsymbol{F}_{int}$, $\boldsymbol{F}_{enh}$, $\boldsymbol{F}_{ext}$ are quantities presented in Eqs. (4)–(9). For details on matrices $\boldsymbol{B}$, $\boldsymbol{\Gamma}$, $\boldsymbol{C}$, $\boldsymbol{S}^{mod}$, $\boldsymbol{N}_c$ and vectors $\boldsymbol{b}^*$, $\boldsymbol{t}^*$ the reader can see publication [20].

$$\boldsymbol{K}_{uu} = \int_{V_0} \boldsymbol{B}^T \boldsymbol{C} \boldsymbol{B} dV \tag{4}$$

$$\boldsymbol{K}_{au} = \int_{V_0} \boldsymbol{\Gamma}^T \boldsymbol{C} \boldsymbol{B} dV \tag{5}$$

$$\boldsymbol{K}_{aa} = \int_{V_0} \boldsymbol{\Gamma}^T \boldsymbol{C} \boldsymbol{\Gamma} dV \tag{6}$$

$$\boldsymbol{F}_{int} = \int_{V_0} \boldsymbol{B}^T \boldsymbol{S}^{mod} dV \tag{7}$$

$$\boldsymbol{F}_{enh} = \int_{V_0} \boldsymbol{\Gamma}^T \boldsymbol{S}^{mod} dV \tag{8}$$

$$\boldsymbol{F}_{ext} = \int_{V_0} \boldsymbol{N}_c^T \boldsymbol{b}^* dV + \int_{A_\sigma} \boldsymbol{N}_c^T \boldsymbol{t}^* dV \tag{9}$$

2.2 Contact FE Formulation

The last integral in Eq. (1) over the contact area C_c denotes the normal contact contribution. For the frictionless case the normal traction is described in Eq. (10).

$$\begin{aligned} \int_S e_N g_n \delta g_n ds = & \int_S e_N (\delta \boldsymbol{r}_S - \delta \boldsymbol{\rho}) \cdot (\boldsymbol{n} \otimes \boldsymbol{n})(\boldsymbol{v}_S - \boldsymbol{v}) ds \\ & - \int_S N a^{ij} (\delta \boldsymbol{\rho}_{,j} \cdot (\boldsymbol{n} \otimes \boldsymbol{\rho}_i)(\boldsymbol{v}_S - \boldsymbol{v}) + (\delta \boldsymbol{r}_S - \delta \boldsymbol{\rho}) \cdot (\boldsymbol{\rho}_j \otimes \boldsymbol{n}) \boldsymbol{v}_{,i}) ds \\ & - \int_S e_N g (\delta \boldsymbol{r}_S - \delta \boldsymbol{\rho}) \cdot h^{ij} (\boldsymbol{\rho_i} \otimes \boldsymbol{\rho_j})(\boldsymbol{v}_S - \boldsymbol{v}) ds \end{aligned} \tag{10}$$

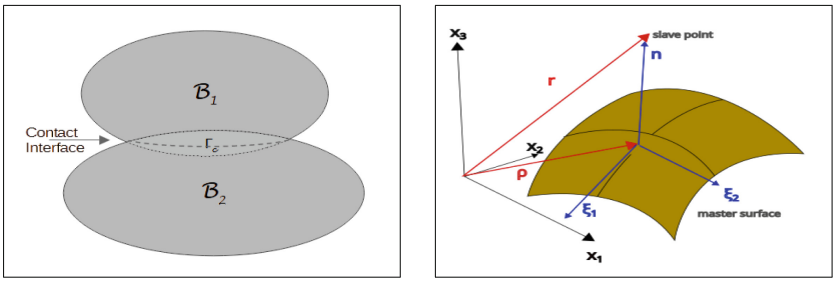

(a) Interface (b) Master surface and slave point

Fig. 1: Contact conditions

Where e_N the penalty factor, $\boldsymbol{r}_S$ and $\boldsymbol{\rho}$ the slave and master surface vectors respectively as shown in Fig. 4b, $\boldsymbol{v}_S$ and $\boldsymbol{v}$ the slave and master surfaces velocities, $\boldsymbol{n}$ the surface normal vector, N the contact normal traction or contact force, h^{ij} the curvature tensor, a^{ij} the contravariant components of the metric tensor, g the measured penetration.

The first step before calculating all contact related quantities is to measure the interfacial gap as presented in Eq. (11).

$$g = (\boldsymbol{r}_S - \boldsymbol{\rho}) \cdot \boldsymbol{n} \tag{11}$$

The gap can be measured between two points defined in the slave and master surfaces. The point on the slave surface is predefined during the analysis and can be either a node or a Gauss point depending on the contact formulation. In Surface to Surface formulation it is usually a Gauss point and its coordinates are already known. The point on the master surface though, is not defined a priori. The Closest Point Projection or CPP method must be implemented to calculate the coordinates of the projected point on the master surface. Since the surface is not linear a Newton procedure is followed. Each increment is calculated based on Eq. (12).

$$\boldsymbol{\xi}^{n+1} = \boldsymbol{\xi}^n + \boldsymbol{\Delta\xi}^{n+1} \tag{12}$$

Where $\Delta\boldsymbol{\xi}^{n+1}$ is calculated as shown in Eq. (13). The reader can find details on the $(\boldsymbol{F}''^{-1})^n$ and $(\boldsymbol{F}')^n$ quantities in [21].

$$\Delta\xi^{n+1} = \begin{bmatrix} \Delta\xi_1^{n+1} \\ \Delta\xi_2^{n+1} \end{bmatrix} = -(\boldsymbol{F}''^{-1})^n (\boldsymbol{F}')^n \tag{13}$$

The matrix formulation for contact elements based on the Surface to Surface formulation is given in [22] and presented in current paper in Eq. (14) for the stiffness matrix and Eq. (15) for the related residual vector.

$$\boldsymbol{K}_{contact} = \boldsymbol{K}_{main} + \boldsymbol{K}_{rot} + \boldsymbol{K}_{curv} \tag{14}$$

$$\boldsymbol{R} = -e_N \xi^3 \boldsymbol{A}^T \boldsymbol{n} \tag{15}$$

where quantities $\boldsymbol{K}_{main}$, $\boldsymbol{K}_{rot}$ and $\boldsymbol{K}_{curv}$ are presented in Eqs. (16), (17) and (18) respectively.

$$\boldsymbol{K}_{main} = e_N H(-\xi^3)\boldsymbol{A}^T(\boldsymbol{n} \otimes \boldsymbol{n})\boldsymbol{A} \tag{16}$$

$$\boldsymbol{K}_{rot} = e_N H(-\xi^3)\xi^3 \left[\boldsymbol{A}_{,j}^T a^{ij}(\boldsymbol{n} \otimes \boldsymbol{\rho}_{,i})\boldsymbol{A} + \boldsymbol{A}^T(\boldsymbol{\rho}_{,i} \otimes \boldsymbol{n})a^{ij}\boldsymbol{A}_{,j}\right] \tag{17}$$

$$\boldsymbol{K}_{curv} = e_N H(-\xi^3)\xi^3 \boldsymbol{A}^T(\boldsymbol{\rho}_{,i} \otimes \boldsymbol{\rho}_{,j})h^{ij}\boldsymbol{A} \tag{18}$$

Where $H(-\xi^3)$ the Heaviside function, $\boldsymbol{A}$ the position matrix. More details regarding quantities presented in Eqs. (10), (15) and (16)–(18) can be found in [21]. As shown in previous equations, the tangent matrix can be split into three parts. The main part, the rotational part and the curvature part. The first part is the most crucial and the one which handles the normal contact between two surfaces. The rotational part describes potential rotation of the contact surface, and the curvature part essentially describes potential changes on the curvature of the contact surface. Contact parts as described previously need to be calculated on each iteration. For this procedure Algorithm 1 is used.

Algorithm 1 Contact algorithm

```
i ⟶ n − iterations
CPP to calculate projection points          ▷ As presented in Eq. 12
Calculate penetration g                     ▷ As presented in Eq. 11
if g ≤ 0 then
    Calculate K_N                           ▷ As presented in Eq. 14
    Form total K
    Calculate residual R                    ▷ As presented in Eq. 15
else
    Exit loop
end if
Exit loop
```

2.3 Time Discretization

For time discretization the Newmark scheme was implemented based on the original publication [23] which solves the hyperbolic Eq. (19). In the present work, any potential damping effects have been neglected.

$$\boldsymbol{M}\ddot{\boldsymbol{U}}^{t+\Delta t} + \boldsymbol{K}\boldsymbol{U}^{t+\Delta t} = \boldsymbol{\mathcal{R}}^{t+\Delta t} \tag{19}$$

For the solution of such a system an incremental approach is used. In each increment, the effective loads $\boldsymbol{\mathcal{R}}^{t+\Delta t}$ along with the displacement vector $\boldsymbol{U}^{t+\Delta t}$ and acceleration vectors $\ddot{\boldsymbol{U}}^{t+\Delta t}$ are calculated. The reader can find a concise explanation of all related quantities in [24] as well as in Newmark's original publication.

2.4 Energy Absorption

The most common energy-based metrics to assess automotive parts crashworthiness are specific energy absorption (SEA) and energy absorption (EA) ([25], [26]). Energy absorption during crashing is formulated as Eq. (20)

$$EA = \int_0^s F(u)du \tag{20}$$

where s denotes the crash displacement and F denotes the impact force. SEA denotes the energy absorbed per unit mass of the absorber, which can be calculated as:

$$SEA = \frac{EA}{M} \tag{21}$$

with M denoting the mass of the structure.

3 Multiscale Analysis and Surrogate Modeling

In order to study the performance of car bumbers made of CNT-reinforced polymers in terms of their crashworthiness and their capacity for energy absorption, a detailed numerical model has been developed based on the FE^2 multiscale finite element method, which is appropriately customized to take into account the mechanical interactions between CNTs and the polymeric host material.

Starting from the nanoscale, a single CNT can be described as an assembly of covalent bonds developed between the carbon atoms (C-C bond) in hexagonal shapes (Fig. 2a). In the context of the molecular structural mechanics approach (MSM) [27], CNTs are seen as space frames where the carbon atoms represent the nodes and the C-C bonds the structural elements (i.e. beams) that connect them. Although this structural representation is a straightforward and accurate transition from the molecular mechanics, the complexity of the system persists, since each space frame that simulates a CNT is inherently defined by an enormous amount of Degrees Of Freedom (DOFs). To be able to efficiently incorporate the CNTs in the microstructure modelling, a further simplification is done. This is performed in a similar manner to the MSM approach with the projection of each space frame structure onto an equivalent beam element(EBE) [28] with the relations:

$$(EA)_{eq}^{EBE} = \frac{F_x L^{SF}}{u_x} \tag{22a}$$

$$(EI)_{eq}^{EBE} = \frac{F_y (L^{SF})^3}{3u_y} \tag{22b}$$

$$(GJ)_{eq}^{EBE} = \frac{TL^{SF}}{\varphi} \tag{22c}$$

where the axial stiffness $(EA)_{eq}^{EBE}$, the bending rigidity $(EI)_{eq}^{EBE}$ and the torsional rigidity $(GJ)_{eq}^{EBE}$ of the EBE, are obtained by measuring the horizontal

displacement u_x, the vertical displacement u_y and the angle of rotation φ that emerge from the imposed loads (i.e. axial force F_x, shear force F_y and torsion T) on the space frame of length L^{SF}.

At the microscale scale level, we consider a representative volume element (RVE) of the composite material which consists of polymer as the host material and randomly scattered EBEs inside it (Fig. 2b) . To simulate the interaction between the CNTs and the cement paste, the embedding finite element technique is implemented according to [29]. Based on this approach, the complete stiffness matrix of the whole system's interaction is:

$$\boldsymbol{K}_{micro} = \boldsymbol{K}_s + \sum_{i=1}^{N} \boldsymbol{K}_{b_i}^{'} \tag{23}$$

where $\boldsymbol{K}_s$ is the solid stiffness matrix, while $\boldsymbol{K}_{b_i}^{'}$ is the stiffness matrix of the i^{th} EBE for a system of N total EBEs.

Lastly, at the macroscale we consider the finite element model of a car bumper, which is described by a homogeneous material with a constitutive relation formulated by the coupling with the previous scale (Fig. 2c). This coupling is achieved with a standard computational homogenization scheme where the macroscopic stress vector $\boldsymbol{\sigma}^M$ and the tangent modulus $\boldsymbol{C}^M$ are obtained after averaging over the microscopic stress field $\boldsymbol{\sigma}^m$ that is developed within the RVE for prescribed boundary conditions according to the following equations:

$$\boldsymbol{\sigma}^M = \frac{1}{\|\Omega\|} \int_{\|\Omega\|} \boldsymbol{\sigma}^m d\Omega \tag{24}$$

$$\boldsymbol{C}^M = \frac{1}{\|\Omega\|} \frac{\partial \int_{\|\Omega\|} \boldsymbol{\sigma}^m d\Omega}{\partial \boldsymbol{\epsilon}^M} \tag{25}$$

where $\|\Omega\|$ denotes the volume of the RVE's domain Ω.

In the context of the FE^2 solution scheme, the constitutive law of the composite material at each integration point of the macroscale FE model is given from Eqs. (24) and (25). Then, the macroscopic quantities $\boldsymbol{\sigma}^M$ and $\boldsymbol{C}^M$ are used in Eqs. (4)–(9) to calculate the stiffness matrices for the composite and the internal force vectors. The issue with this approach, however, is that at each integration point, one needs to solve an RVE boundary value problem for prescribed macroscopic strains $\boldsymbol{\epsilon}^M$ in order to retrieve the microscopic stress field $\boldsymbol{\sigma}^m$, which will be later averaged to get $\boldsymbol{\sigma}^M$. This results in an enormous computational cost, especially for detailed FE models that contain a large number of integration points.

To alleviate this computational burden, the idea has been proposed in [18,29] and employed herein, to utilize feedforward neural networks that learn the stress-strain (input-output) relation of the RVE based on a limited set of RVE analyses, as schematically depicted in Fig. 3. To construct the training data set, N RVEs are solved via FEM for different strain combinations $\{\boldsymbol{\epsilon}_i^M\}_{i=1}^N$ and the corresponding macroscopic stresses $\{\boldsymbol{\sigma}_i^M\}_{i=1}^N$ are computed. A feedforward neural

network is then tasked to learn the relation and predict the macroscopic stress for a given macroscopic strain. The tangent modulus $\boldsymbol{C}^M$ is straightforwardly computed using automatic differentation. With this approach, the NN mimics the composite material's behavior and effectively overcomes the need for solving the RVE boundary value problem, resulting in drastic cost reduction.

(a) Nanoscale: A single CNT modelled as an equivalent beam element

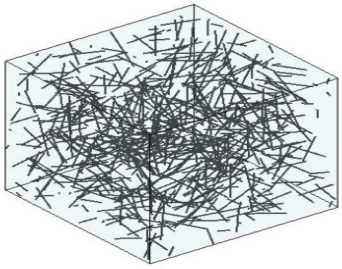

(b) Microscale: A RVE of the CNT reinforced polymer

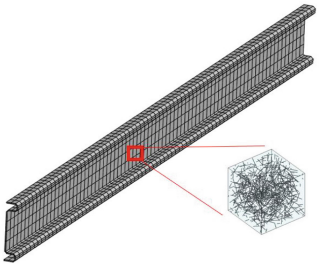

(c) Macroscale: Car bumper made up from CNT-reinforced polymer

Fig. 2: Distinct scales in the multiscale problem

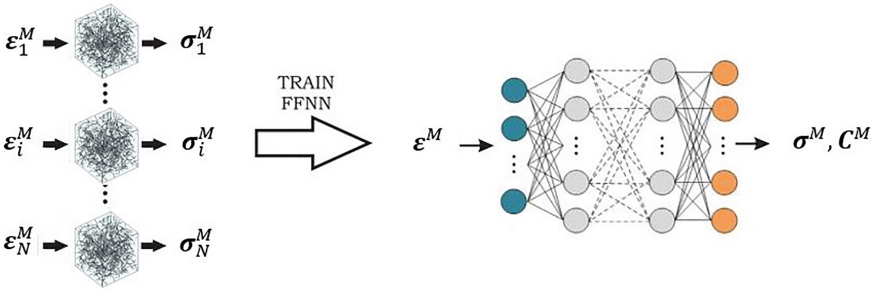

Fig. 3: Surrogate modeling strategy to train NNs that mimic the RVE's strain-stress relation

4 Numerical Application

The computational tools developed in the previous sections are utilized in a real-life application of a rear truck bumper colliding with a rigid impactor. A 3D finite element model has been developed for the description of impact of the bumper with the impactor (Fig. 4a). The bumper is made of PEEK material, where the Young's modulus is set to $E = 3.5$ GPa and the Poisson's ratio to 0.40, assuming a bi-linear elastic-plastic material model with 30% hardening ratio. The PEEK density is 1320 kg/m^3. A cylindrical impactor with height and radius of 0.20 m and a 12 kg mass hits the middle section of the bumper with an initial velocity of 25 km/h . For the boundary conditions of the model, fixed supports were placed on all the nodes of the rear side of the bumper in contact with the truck brackets as shown in Fig. 4b. Figure 5a and b depict two views of the finite element mesh for the two bodies in contact.

Table 1: Finite element mesh statistics

	Type of element	Number of nodes Dof	Number of elements
Bumper	Solid Shell	3726/11178	1760
Impactor	Hexa8	1408/4224	1060
Contact elements	Surface – to – Surface	(–)	3712
Total		5134/15402	6532

For the bumper mesh, Solid Shell elements with 7 internal degrees of freedom were used, while the impactor was meshed using 8-noded Hexahedron elements. For the contact interaction frictionless Surface – to – Surface elements based on the penalty formulation were utilized. Without the application of a more efficient collision detection algorithm, a set of predefined master surfaces candidates located on the potential contact zone of the bumper is paired with a set of slave surfaces located on the potential contact zone of the impactor and the closest point projection procedure as well as the evaluation of the respective gap functions is calculated for each pair in order to determine the active contact zone in each time increment and iteration of the solution process. The finite element mesh statistics of the model are given in Table 1.

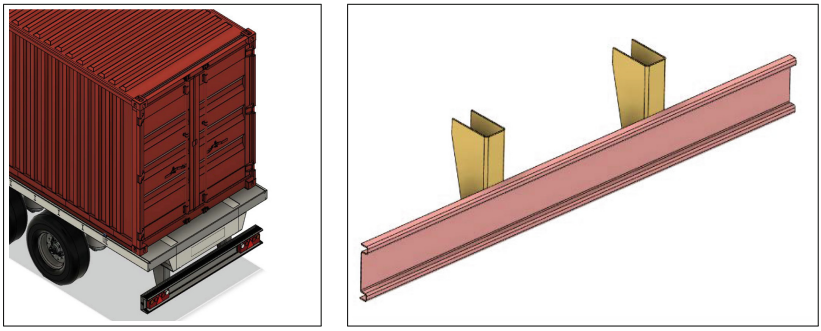

(a) 3-axle truck (b) Bumper with support brackets

Fig. 4: Truck bumper

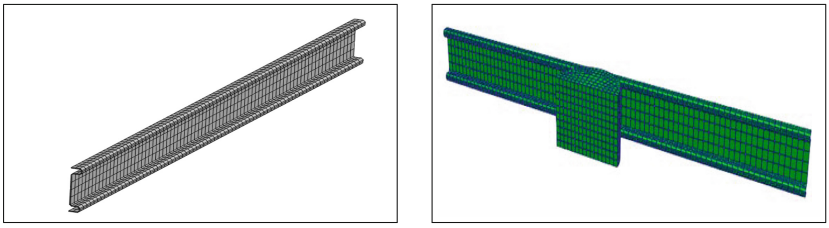

(a) Bumper mesh (b) Bumper and impactor mesh

Fig. 5: Truck bumper mesh

For the composite material 1 case was considered, assuming 1.0$wt.\%$. The obtained results that include comparative diagrams of the maximum deflection of the bumper, the strain energy, the dissipated energy as well as the deformed configuration of the bumper, for the cases of the base PEEK material and the case of 1.0$wt.\%$ CNT-reinforced composite are presented next.

From the results given below it is apparent that the 1.0$wt.\%$ CNT-reinforced PEEK material is stiffer as the maximum displacement displays a reduction of approximately 7.5% (5.74 Vs 6.2 cm). As a result of that, the impact duration also displays a decrease for the CNT-reinforced composite (0.013 Vs 0.0152 s). Finally, the maximum permanent displacement is slightly reduced from 2.87 cm to 2.71 cm.

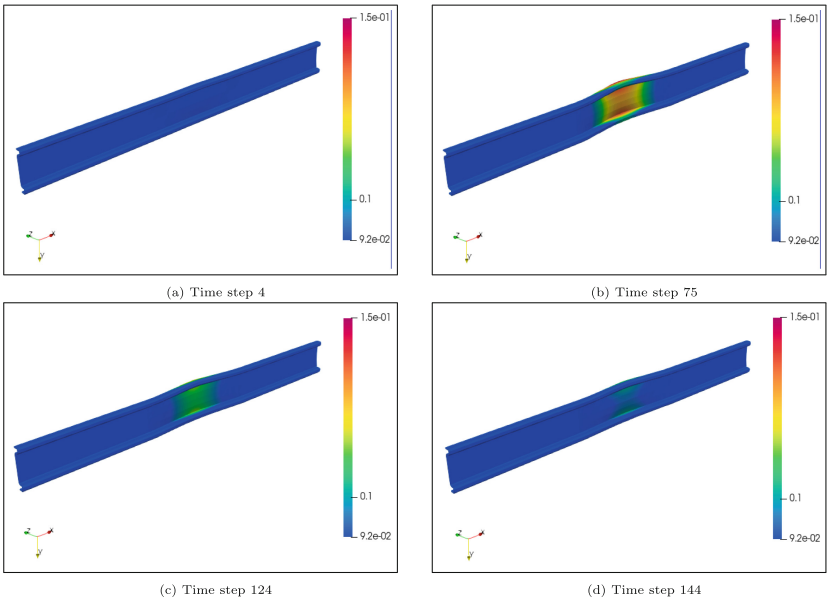

(a) Time step 4 (b) Time step 75

(c) Time step 124 (d) Time step 144

Fig. 6: Resulted displacements for various time steps during the implicit dynamics analysis

From the results we obtained that are given in the last two figures, an increase of the dissipated energy due to plastic deformation is observed, for the same amount of energy absorption of the bumper structure. These results indicate that even for only 1.0$wt.\%$ CNT-reinforcement a significant improvement of the crash-worthiness of the bumper is obtained, as a larger amount of energy is

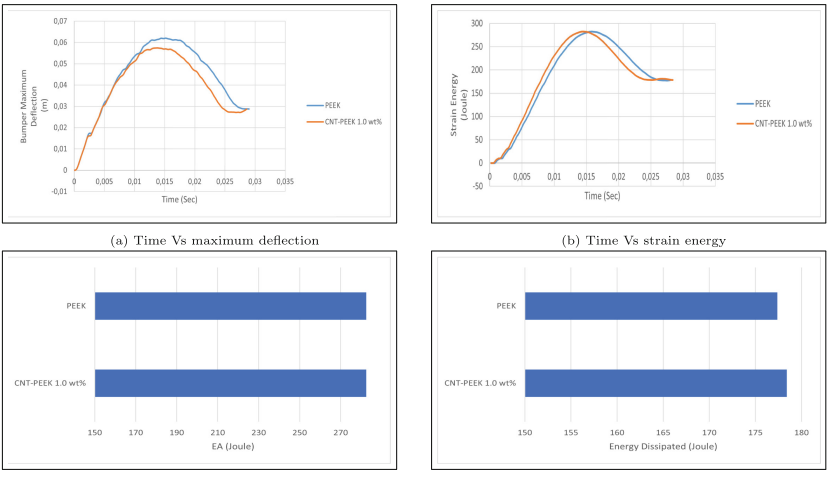

(a) Time Vs maximum deflection (b) Time Vs strain energy

(c) Absorbed energy (d) Dissipated energy

Fig. 7: Results diagrams

dissipated while the bumper's displacements remain lower than in the case with the base PEEK material.

5 Conclusions

In this work, a novel computational model has been developed for the investigation of the behavior of car bumpers made of CNT-reinforced composites in crash scenarios. In particular, the FE^2 multiscale finite element method has been coupled with a dedicated contact finite element formulation, enabling us to solve accurately the partial differential equations that govern the impact problem. Additionally, a surrogate modelling technique has been employed based on artificial neural networks in order to accelerate the computationally demanding FE^2 solution scheme. With these tools at hand, a parametric investigation has been performed to assess the energy absorption properties and crash-worthiness of CNT-reinforced car bumpers for a given weight fractions of CNTs in the polymeric matrix. The results suggest that the addition of CNTs to the material improves the energy absorption of the car bumper system and it is expected that the energy absorption of the bumper system will increase significantly as we increase the weight fraction of CNTs. As a future step, our aim is to validate this hypothesis, and deploy this model on an exascale HPC systems for performing material optimization in order to find the optimal material configurations that will maximize the vehicle's crash-worthiness.

Acknowledgments. This work has been supported by the REGALE project. The REGALE project has received funding from the European High-Performance Computing Joint Undertaking (JU) under grant agreement No 956560. The JU receives support from the European Union's Horizon 2020 research and innovation program and Greece, Germany, France, Spain, Austria, Italy. The REGALE project has also been funded by the German Federal Ministry of Education and Research (BMBF) based on a decision of the German Bundestag.

References

1. Y. Zhang, P. Zhu, G. Chen, Z. Lin, Study on structural lightweight design of automotive front side rail based on response surface method, The Journal of Mechanical Design 129 (5) (2007) 553–557. https://doi.org/10.1115/1.2712223.
2. J. Fang, G. Sun, N. Qiu, N. H. Kim, Q. Li, On design optimization for structural crashworthiness and its state of the art, Structural and Multidisciplinary Optimization 55 (2017) 1091–1119.
3. S. Prabhakaran, K. Chinnarasu, M. S. Kumar, Design and fabrication of composite bumper for light passenger vehicles, International Journal of Modern Engineering Research 2 (4) (2012) 2552–2556.
4. R. Hosseinzadeh, M. M. Shokrieh, L. B. Lessard, Parametric study of automotive composite bumper beams subjected to low-velocity impacts, Composite Structures 68 (4) (2005) 419–427.

5. M. Davoodi, S. Sapuan, D. Ahmad, A. Ali, A. Khalina, M. Jonoobi, Mechanical properties of hybrid kenaf/glass reinforced epoxy composite for passenger car bumper beam, Materials & Design 31 (10) (2010) 4927–4932.
6. S. Berber, Y.-K. Kwon, D. Tománek, Unusually high thermal conductivity of carbon nanotubes, Phys. Rev. Lett. 84 (2000) 4613–4616. https://doi.org/10.1103/PhysRevLett.84.4613. https://link.aps.org/doi/10.1103/PhysRevLett.84.4613.
7. T. W. Ebbesen, H. J. Lezec, H. Hiura, J. W. Bennett, H. F. Ghaemi, T. Thio, Electrical conductivity of individual carbon nanotubes, Nature 382 (1996) 54–56.
8. M. Treacy, T. Ebbesen, J. Gibson, Exceptionally high young's modulus observed for individual carbon nanotubes, Nature 381 (6584) (1996) 678–680. https://doi.org/10.1038/381678a0.
9. W. Liu, L. Li, S. Zhang, F. Yang, R. Wang, Mechanical properties of carbon nanotube/carbon fiber reinforced thermoplastic polymer composite, Polymer Composites 38 (9) (2017) 2001–2008.
10. N. Sapiai, A. Jumahat, J. Mahmud, Mechanical properties of functionalised cnt filled kenaf reinforced epoxy composites, Materials Research Express 5 (4) (2018) 045034.
11. N. Nurazzi, F. Sabaruddin, M. Harussani, S. Kamarudin, M. Rayung, M. Asyraf, H. Aisyah, M. Norrrahim, R. Ilyas, N. Abdullah, et al., Mechanical performance and applications of cnts reinforced polymer composites-a review, Nanomaterials 11 (9) (2021) 2186.
12. Z. Benzait, L. Trabzon, A review of recent research on materials used in polymer-matrix composites for body armor application, Journal of Composite Materials 52 (23) (2018) 3241–3263.
13. A. Alian, S. El-Borgi, S. Meguid, Multiscale modeling of the effect of waviness and agglomeration of cnts on the elastic properties of nanocomposites, Computational Materials Science 117 (2016) 195–204. https://doi.org/10.1016/j.commatsci.2016.01.029. https://www.sciencedirect.com/science/article/pii/S0927025616300027.
14. S. A. Parvin, N. A. Ahmed, A. M. Fattahi, Numerical prediction of elastic properties for carbon nanotubes reinforced composites using a multi-scale method, Engineering with Computers (2020) 1–12.
15. C. Miehe, A. Koch, Computational micro-to-macro transitions of discretized microstructures undergoing small strains, Archive of Applied Mechanics 72 (4–5) (2002) 300–317. https://doi.org/10.1007/s00419-002-0212-2.
16. F. Feyel, A multilevel finite element method (fe2) to describe the response of highly non-linear structures using generalized continua, Computer Methods in Applied Mechanics and Engineering 192 (28) (2003) 3233–3244, multiscale Computational Mechanics for Materials and Structures. https://doi.org/10.1016/S0045-7825(03)00348-7. https://www.sciencedirect.com/science/article/pii/S0045782503003487.
17. I. Kalogeris, S. Pyrialakos, O. Kokkinos, V. Papadopoulos, Stochastic optimization of carbon nanotube reinforced concrete for enhanced structural performance, Engineering with Computers. https://doi.org/10.1007/s00366-022-01693-8.
18. S. Pyrialakos, I. Kalogeris, V. Papadopoulos, Multiscale analysis of nonlinear systems using a hierarchy of deep neural networks, International Journal of Solids and Structures 271–272 (2023) 112261. https://doi.org/10.1016/j.ijsolstr.2023.112261. https://www.sciencedirect.com/science/article/pii/S0020768323001580.
19. R. Hauptmann, K. Schweizerhof, S. Doll, Extension of the 'solid-shell' concept for application to large elastic and large elastoplastic deformations, International Journal for Numerical Methods in Engineering 49 (2000) 1121–1141.

20. N. N. Nguyen, Development of solid-shell elements for large deformation simulation and springback prediction, Computational Mechanics.
21. A. Konyukhov, K. Schweizerhof, Contact formulation via a velocity description allowing efficiency improvements in frictionless contact analysis, Computational Mechanics 33 (2004) 1165–173.
22. R. Izi, A. Konyukhov, K. Schweizerhof, Large penetration algorithm for 3d frictionless contact problems based on a covariant form, Computer Methods in Applied Mechanics and Engineering 217–220 (2012) 186–196.
23. N. M. Newmark, A method for computation of structural dynamics, ASCE Journal of Engineering Mechanics Division 85 (1959) 67–94.
24. K.-J. Bathe, Finite Element Procedures, PHI, 2014.
25. N. S. Muhammad, A. Hambali, J. Rosidah, W. Widodo, M. Ahmad, A review of energy absorption of automotive bumper beam, International Journal of Applied Engineering Research 12 (2) (2017) 238–245.
26. C. W. Isaac, C. Ezekwem, A review of the crashworthiness performance of energy absorbing composite structure within the context of materials, manufacturing and maintenance for sustainability, Composite Structures 257 (2021) 113081.
27. C. Li, T.-W. Chou, A structural mechanics approach for the analysis of carbon nanotubes, International Journal of Solids and Structures 40 (10) (2003) 2487–2499.
28. P. Papanikos, D. Nikolopoulos, K. Tserpes, Equivalent beams for carbon nanotubes, Computational Materials Science 43 (2) (2008) 345–352.
29. S. Pyrialakos, I. Kalogeris, G. Sotiropoulos, V. Papadopoulos, A neural network-aided bayesian identification framework for multiscale modeling of nanocomposites, Computer Methods in Applied Mechanics and Engineering 384 (2021) 113937.